On the proper calculation of electrostatic interactions in solid-supported bilayer systems

In-Chul Yeh[a] and Anders Wallqvist
Biotechnology High Performance Computing Software Applications Institute, Telemedicine and Advanced Technology Research Center, U.S. Army Medical Research and Materiel Command, Fort Detrick, Maryland 21702, USA

(Received 21 September 2010; accepted 6 January 2010; published online 4 February 2011)

Modeling systems that are not inherently isotropic, e.g., extended bilayers, using molecular simulation techniques poses a potential problem. Since these methods rely on a finite number of atoms and molecules to describe the system, periodic boundary conditions are implemented to avoid edge effects and capture long-range electrostatic interactions. Systems consisting of a solvated bilayer adsorbed on a solid surface and exposed to an air/vacuum interface occur in many experimental settings and present some unique challenges in this respect. Here, we investigated the effects of implementing different electrostatic boundary conditions on the structural and electrostatic properties of a quartz/water/vacuum interface and a similar quartz-supported hydrated lipid bilayer exposed to vacuum. Since these interfacial systems have a net polarization, implementing the standard Ewald summation with the conducting boundary condition for the electrostatic long-range interactions introduced an artificial periodicity in the out-of-plane dimension. In particular, abnormal orientational polarizations of water were observed with the conducting boundary condition. Implementing the Ewald summation technique with the planar vacuum boundary condition and calculating electrostatic properties compatible with the implemented electrostatic boundary condition removed these inconsistencies. This formulation is generally applicable to similar interfacial systems in bulk solution. © *2011 American Institute of Physics*. [doi:10.1063/1.3548836]

I. INTRODUCTION

As many chemical, biological, and physiological processes sensitively depend on long-range electrostatic forces, it is essential that the molecular descriptions used to probe these systems correctly account for these forces.[1] Periodic boundary conditions (PBCs) are the natural choice in computer simulations to avoid edge effects due to the finite number of atoms and molecules located in a unit cell.[2] Treatments of electrostatic interactions under PBCs can strongly influence calculated properties and, hence, the physical and biological interpretation of the modeled systems. A number of different methods[3,4] have been implemented for calculating electrostatic interactions in systems described by PBCs. The method of choice, the Ewald summation method,[2,3,5,6] combined with the particle mesh Ewald technique,[7] provides an efficient mean to calculate electrostatic interactions for molecular systems subject to PBCs and has been broadly implemented in biomolecular simulation studies.[8] Solid-supported lipid bilayer films exposed to an air/vacuum interface have been studied extensively experimentally[9] and computationally.[10,11] However, the implementation of the Ewald sum in such nonisotropic systems presents some unique problems. An improper consideration of electrostatic boundary conditions for such systems can result in nonphysical artifacts.[12,13] Here, we present an implementation of the electrostatic boundary condition that includes a straightforward correction term to remove these artifacts.

The Ewald summation formula contains a surface term that depends on the dielectric constant of the medium surrounding the periodic images.[2,5,14,15] This surface term vanishes for the conducting boundary condition where the dielectric constant of the surrounding medium is infinite.[2,5] However, for vacuum boundary conditions where the surrounding medium is characterized by a dielectric constant of 1, the surface term is expressed as a function of the total dipole moment or polarization of the system.[2,5] The surface term has a slightly different functional form depending on the order or mode of summation.[14,15] It plays an important role in modeling molecular systems that are not inherently isotropic, e.g., extended bilayers, or polarized interfacial systems.[16] For systems with planar interfaces, the planar vacuum boundary condition where periodic images are surrounded by planar vacuum boundaries would be a natural choice. For this boundary condition, the Ewald summation is carried out in the planar manner, i.e., summing in planar directions first and then progressing in the out-of-the plane direction. The resulting surface term depends only on the total dipole moment in the out-of-the plane direction.[14] Yeh and Berkowitz[16] demonstrated that simulations with the surface term corresponding to the planar vacuum boundary condition in conjunction with an extra vacuum space along the out-of-the plane direction reproduce results obtained by the rigorous, but computationally expensive, two-dimensional Ewald summation technique[17] almost exactly. This approximation holds as long as the length of the extra vacuum space along the out-of-the plane direction is longer than the periodic box lengths in planar directions.[16] Subsequently, simulations of

[a]Author to whom correspondence should be addressed. Electronic mail: icy@bioanalysis.org.

many interfacial systems have successfully implemented this surface term for the planar vacuum boundary condition.[18,19] However, the vast majority of molecular dynamics (MD) simulations are still being performed with the conducting boundary condition regardless whether the simulated system has a net polarization or not. Thus, it is important to highlight the consequence of using conducting boundary conditions in simulations of systems with nonzero net polarization.

It is important when simulations are performed using a specific electrostatic boundary condition that the calculations of electrostatic properties are consistent with the implemented boundary condition. Sachs *et al.*[20] and Yeh and Hummer[21] introduced an accurate formula to calculate the electrostatic potential profile from simulations performed with the conducting boundary condition. This formula includes a previously overlooked integration constant, which is necessary to enforce the three-dimensional (3D) PBC. Interestingly, as will be shown below, this integration constant has the same functional form as the surface term for the planar vacuum boundary condition but with an opposite sign. As a result, the traditional formula for calculating the electrostatic potential without the integration constant was found to be appropriate for simulations performed with the planar vacuum boundary condition.

Earlier considerations of the planar vacuum boundary did not specifically address the systems considered here, in particular, those with intrinsically isotropic components mixed with a strongly polarized local component. These systems with nonzero net polarization are encountered even in the absence of charged surfaces or external electric fields, e.g., in net-neutral asymmetric lipid bilayers or quartz crystal microbalance measurements performed on polarized crystals.[22] In this report, we examined the structural and electrostatic properties of interfacial systems with nonzero net polarization calculated with different electrostatic boundary conditions. We observed abnormal orientational polarizations of water in simulations of a quartz/water interface and a similar quartz-supported hydrated dimyristoylphosphatidylcholine (DMPC) bilayer embedded in vacuum, performed while using the standard Ewald summation with the conducting boundary condition. Implementing the Ewald summation technique with the planar vacuum boundary condition removed these abnormal polarizations of water. Here, we give the correct formulas for obtaining electrostatic properties consistent with different boundary conditions. We also confirmed that the modeled quartz-supported hydrated lipid bilayer reproduced the essential features of the lipid bilayer in bulk water. Finally, we showed that the planar vacuum boundary condition can be applied to bulk phase simulations of a quartz/water interface in order to remove artifacts introduced by the conducting boundary condition.

II. METHODS

A. Simulations

MD simulations were performed with the NAMD MD simulation program[23] and CHARMM all atom force field[24] for DMPC. The TIP3P water model[25] was used to describe water molecules. The force field for a quartz (011) crystal was taken from the one developed by Lopes *et al.*[26] A primitive unit cell of quartz (011) of ~15-Å thickness was replicated in two dimensions to construct a quartz (011) crystal with a surface area of 36.5 × 37.0 Å^2, as in the previous study by Lopes *et al.*[26] One side of the constructed crystal was covered with hydrophilic silanols (Si–OH), and silicon atoms on the other side were saturated with hydrogens (Si–H). Crystal atoms, except for the O–H groups of silanols, were held fixed to maintain the (011) crystal geometry. Simulations of the quartz/water interface and the quartz-supported lipid bilayer embedded in vacuum were performed with fixed simulation box sizes using 3D PBCs. However, the box length (L_z) in the z-direction normal to the interface was chosen to be large enough for the system to form interfaces with the vacuum. This allowed the systems to adjust to an optimum density without constant pressure simulations. The penetration of water molecules into the vacuum phase was negligible under all systems and conditions studied in this work. Short-range interactions outside a 10-Å cutoff were truncated. Long-range electrostatic interactions were calculated with the particle mesh Ewald method with and without the surface term for the planar vacuum boundary condition,[16] referred to as EW3DC and EW3D, respectively. The EW3D method is equivalent to implementing the Ewald summation with the conducting boundary condition. The contribution to the potential energy (U_c) from the EW3DC correction term is given by the following surface term for the planar vacuum boundary condition:

$$U_c = \frac{1}{4\pi\varepsilon_0}\frac{2\pi}{V}M_z^2 = \frac{1}{2\varepsilon_0 V}M_z^2, \tag{1}$$

where ε_0, V, and M_z are the vacuum permittivity, the volume of the unit simulation cell, and the z-component of the total dipole moment of the unit simulation cell. The contribution to the force ($F_{z,i}$) acting on atom i with an electrostatic charge of q_i from this term is as follows:

$$F_{z,i} = -\frac{\partial U_c}{\partial z_i} = -\frac{q_i}{\varepsilon_0 V}M_z. \tag{2}$$

We implemented the EW3DC correction term in NAMD by adding forces due to the following effective electric field (E^{EW3DC}) in the z-direction[16]:

$$E^{\mathrm{EW3DC}} = -\frac{M_z}{\varepsilon_0 V}. \tag{3}$$

This electric field can also be related to the z-component of polarization (P_z) as follows:

$$E^{\mathrm{EW3DC}} = -\frac{P_z}{\varepsilon_0}. \tag{4}$$

Bonds involving hydrogens were constrained with the SHAKE algorithm.[27] A time step of 2 fs was used for the time integration. The temperature was maintained at 310 K using Langevin dynamics with a damping coefficient of 10 ps^{-1}.[28] Coordinates were saved at every 1 ps for further analysis. Errors reported in this work were based on the 95% confidence interval estimated as 1.96 times the standard error.

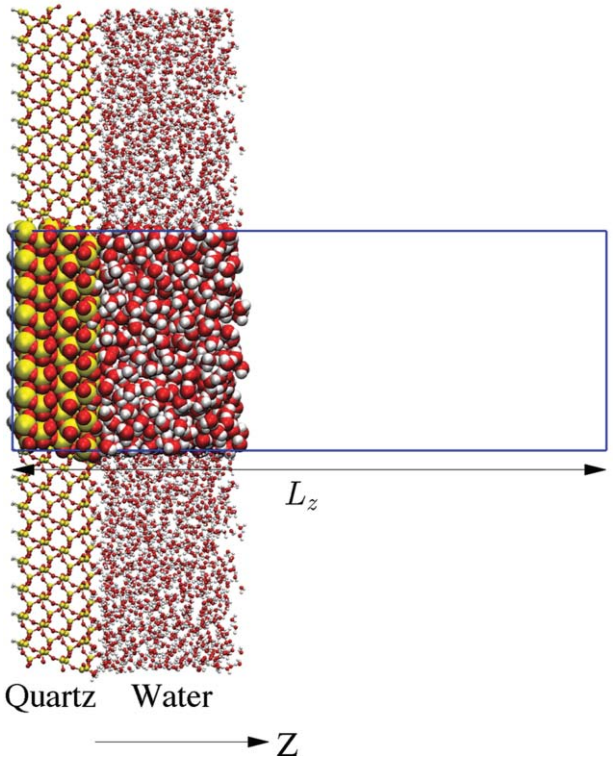

FIG. 1. A snapshot from the simulation of a quartz/water interface embedded in vacuum. The blue box represents the unit simulation cell with a box length in the z-direction (L_z) of 100 Å. The simulation cell is repeated periodically in all three directions. Water is in contact with the hydrophilic side of the quartz (011). Empty space (vacuum) is used to separate water and the other side of the quartz crystal in the z-direction.

Standard errors were estimated from an analysis of five equal time blocks from the trajectory of each production run.

B. Quartz/water interface

A quartz/water interface was prepared by adding 985 water molecules to the hydrophilic side of the crystal. Four simulations with different L_z values of 100, 150, 200, and 300 Å were performed with the EW3D method. The smallest box length L_z of 100 Å was used for a simulation with the EW3DC method. A snapshot of the prepared quartz/water system for a L_z of 100 Å is shown in Fig. 1. A water/vacuum interface was formed due to the extra empty space between water and the other side of the crystal in the simulation cell. Figure 1 shows that the length of the extra empty space in the simulation cell with the smallest box length is clearly larger than lateral box lengths, which is required for the successful application of the EW3DC method to effectively remove the periodicity in the z-direction.[16] Each simulation lasted for 20 ns, of which the initial 1 ns was treated as an equilibration period and discarded.

C. Quartz-supported lipid bilayer

A hydrated lipid bilayer composed of 44 DMPC molecules (22 molecules on each leaflet) and 1400 water molecules was prepared in the simulation cell of a rectangular

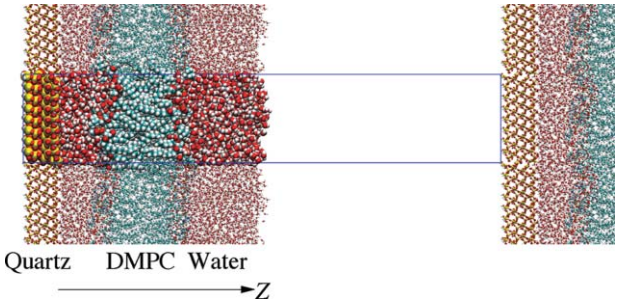

FIG. 2. A snapshot from the simulation of a hydrated dimyristoylphosphatidylcholine (DMPC) lipid bilayer deposited on a quartz crystal surface. The blue box represents the unit simulation cell with L_z of 200 Å. The simulation cell is repeated periodically in all three directions.

prism with the CHARMM-GUI Membrane Builder.[29] The surface area of the rectangular base of the simulation cell was chosen to be same as the area of the quartz (011) surface so that the area per lipid headgroup was ~60 Å^2, close to the experimental value for DMPC.[30] The prepared hydrated DMPC bilayer was equilibrated under NPAT (constant normal pressure and constant lateral surface area of the bilayer and constant temperature) condition with the CHARMM MD simulation program.[31] After a brief run under the same NPAT ensemble with NAMD, the lateral periodic boundaries were gradually changed to those of the quartz (011) surface. The resulting hydrated lipid bilayer was brought closer to the quartz (011) surface, and the thickness of the water layer that interfaces with the membrane and vacuum was doubled. Figure 2 shows the snapshot from MD simulation with this setup. Both the EW3D and EW3DC methods were used to calculate electrostatic interactions. The same L_z of 200 Å was used in both methods. Figure 2 shows that the length of the vacuum region with L_z of 200 Å was clearly larger than lateral box lengths. Each simulation lasted for 200 ns, of which the initial 70 ns was discarded due to equilibration considerations. To investigate possible finite system-size effects, we performed an additional 100-ns simulation with the EW3DC method, where the system size was quadrupled to have 176 lipids by duplicating the simulation system along each of two lateral dimensions. The value for L_z was increased to 250 Å to ensure that the length of the empty space in z-direction is greater than the increased lateral box sizes. Similarly, simulation of a DMPC bilayer in bulk water under the NPAT ensemble with the increased system size was also performed for 100 ns to compare properties of the lipid bilayer in bulk solution and near a polarized quartz interface. The initial 30 ns of these simulations was discarded as equilibration.

D. Quartz/water interface in bulk solution

We prepared a quartz/water interface in bulk solution without vacuum boundaries by adding 1400 water molecules to both the hydrophilic and hydrophobic sides of the quartz (011) crystal. In addition to the O–H groups on the hydrophilic side, hydrogen atoms on the hydrophobic side of the crystal in contact with water were allowed to move. Simulations were performed for 20 ns under the NPAT ensemble.

The initial 1 ns was discarded as equilibration. We used both the conducting boundary condition with the EW3D method and the planar vacuum boundary condition with the EW3DC method to highlight the physical effects introduced by the choice of boundary condition.

E. Electrostatic property profiles across the interface

Distributions of the electrostatic potential and electric field along the z-direction were calculated from the charge density distribution $\rho_q(z)$ obtained from the simulations. Expressions for calculating the electrostatic properties were different depending on the electrostatic boundary condition used in the simulations. First, let us consider the case when the conducting boundary condition was applied as in the EW3D method. Starting from Poisson's equation,

$$\frac{d^2\phi(z)}{dz^2} = -\frac{\rho_q(z)}{\varepsilon_0}, \tag{5}$$

where $\phi(z)$ is the electrostatic potential at position z. An electric field $[E(z)]$ was calculated by integrating Poisson's equation once, as follows:

$$E(z) = -\frac{d\phi(z)}{dz} = \frac{\int_{-L_z/2}^{z} \rho_q(z')dz'}{\varepsilon_0} + C_1, \tag{6}$$

where C_1 is an integration constant. Sachs *et al.*[20] and Yeh and Hummer[21] showed that this integration constant is not necessarily zero but can be determined by enforcing PBCs. Integrating the above equation once more, we obtained the following expression for the electrostatic potential:

$$\phi(z) = -\frac{1}{\varepsilon_0}\int_{-L_z/2}^{z}(z-z')\rho_q(z')dz' - C_1\left(z+\frac{L_z}{2}\right) + C_2. \tag{7}$$

If we choose $z = -L_z/2$ as a reference point and set $\phi(-L_z/2) = 0$, the integration constant C_2 becomes 0. Imposing PBCs by setting $\phi(-L_z/2) = 0 = \phi(-L_z/2 + L_z) = \phi(L_z/2)$ yielded the following expression for C_1:

$$C_1 = -\frac{1}{\varepsilon_0 L_z}\int_{-L_z/2}^{L_z/2}\left(\frac{L_z}{2} - z'\right)\rho_q(z')dz'. \tag{8}$$

Equation (8) was expanded to give the following:

$$C_1 = -\frac{1}{2\varepsilon_0}\int_{-L_z/2}^{L_z/2}\rho_q(z')dz' + \frac{1}{\varepsilon_0 L_z}\int_{-L_z/2}^{L_z/2} z'\rho_q(z')dz'. \tag{9}$$

The first term vanishes because the net charge of the system is zero. Then,

$$C_1 = \frac{1}{\varepsilon_0 L_z}\int_{-L_z/2}^{L_z/2} z'\rho_q(z')dz' = \frac{1}{\varepsilon_0 A L_z}\int_{-L_z/2}^{L_z/2} z'\rho_q(z')Adz' = \frac{M_z}{\varepsilon_0 V} = \frac{P_z}{\varepsilon_0}. \tag{10}$$

By substituting $C_1 = P_z/\varepsilon_0$ into Eqs. (6) and (7), we obtained the following expressions:

$$E(z) = \frac{\int_{-L_z/2}^{z}\rho_q(z')dz'}{\varepsilon_0} + \frac{P_z}{\varepsilon_0}, \tag{11}$$

$$\phi(z) = -\frac{1}{\varepsilon_0}\int_{-L_z/2}^{z}(z-z')\rho_q(z')dz' - \frac{P_z}{\varepsilon_0}\left(z+\frac{L_z}{2}\right). \tag{12}$$

Similar expressions were recently obtained by Gurtovenko and Vattulainen.[32] In their study, they examined the electrostatic potential calculated for asymmetric lipid bilayers with nonzero net polarization using the conducting boundary condition.[32] For this case, they suggested that calculations of the electrostatic potential should be done using formulas appropriate for the planar vacuum boundary condition. However, Eqs. (11) and (12) should be used to calculate electrostatic properties from simulations performed using the EW3D method under the *conducting boundary condition*, regardless of whether the system is polarized or not, as we will show in Sec. III. However, when using the EW3DC method under the *planar vacuum boundary condition*, the P_z/ε_0 term in Eq. (11) is cancelled out at every time step by the effective electric field E^{EW3DC} of the same magnitude but with the opposite sign. Therefore, the following expressions for the electric field and electrostatic potential should be used instead:

$$E(z) = \frac{\int_{-L_z/2}^{z}\rho_q(z')dz'}{\varepsilon_0}, \tag{13}$$

$$\phi(z) = -\frac{1}{\varepsilon_0}\int_{-L_z/2}^{z}(z-z')\rho_q(z')dz'. \tag{14}$$

Equations (13) and (14) are thus appropriate for the EW3DC method using the *planar vacuum boundary condition*.

III. RESULTS AND DISCUSSION

A. Quartz/water interface

1. Structural properties

Figure 3(a) shows a comparison of mass density distributions of water along the z-direction using different electrostatic boundary conditions and box lengths. Overall, these distributions were insensitive to changes in the boundary conditions or box lengths used in the simulations. In all cases, the water density at ~10 Å away from the quartz/water interface at $z = 0$ Å was close to the bulk water density of 0.993 g/cm^3 at 310 K, demonstrating that a well-defined and stable quartz/water interface was formed with the addition of the water/vacuum interface. However, simulations using smaller box lengths with the EW3D method resulted in slightly lower water densities (see Table I). Small differences in water density also existed near the water/vacuum interface. Lopes *et al.*[26] obtained similar water density distributions near the quartz/water interface from simulations of water enclosed between quartz surfaces. The distributions are also similar to those obtained by Wander and Clark[33] using different force field parameters representing the quartz/water interface.

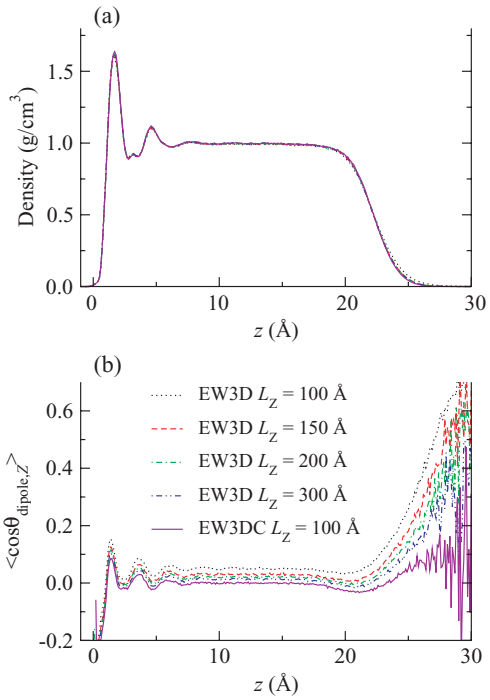

FIG. 3. Structural properties of the quartz/water interface. (a) Distributions of mass density of water under different electrostatic boundary conditions. (b) Average values of cosine of the angle between the water dipole and the z-axis ($\langle\cos\theta_{dipole,z}\rangle$) across the interface.

The average cosine of the angle between the water dipole and the z-axis ($\langle\cos\theta_{dipole,z}\rangle$) is a good indicator of orientational polarizations of water and is sensitive to the choice of electrostatic boundary conditions used in the simulations.[13,34] Figure 3(b) shows $\langle\cos\theta_{dipole,z}\rangle$ of water as a function of the distance from the quartz surface. Under isotropic conditions, as in bulk water without any external electric field, $\langle\cos\theta_{dipole,z}\rangle$ is expected to be zero. In previous simulations of water in contact with solid surfaces using the EW3DC method, the water phase became isotropic roughly 10 Å away from the surface.[18,35] The value of $\langle\cos\theta_{dipole,z}\rangle$ at the region of bulklike water density (10 Å $< z <$ 15 Å) was close to zero with the EW3DC method but was larger than zero for simulations with the EW3D method. These abnormal orientational polarizations of water with the EW3D method were more pronounced at the water/vacuum interface, where the water density was low. The results shown in Fig. 3(b) and Table I show that even though the difference between water orientation distributions decreased with increasing L_z values in the EW3D simulations, noticeable differences persisted even for large L_z values. This indicates that there were significant differences in electrostatic forces experienced by water molecules in simulations with the EW3D and EW3DC protocols.

TABLE I. Values of $\langle\cos\theta_{dipole,z}\rangle$ and the average mass density at the bulklike region (10 Å $< z <$15 Å) of water in the quartz/water interface as a function of different electrostatic boundary conditions and box size variations in the z-direction (L_z).

Electrostatic boundary condition	L_z (Å)	$\langle\cos\theta_{dipole,z}\rangle$	Density (g/cm^3)
EW3D	100	0.0506 (0.0001)	0.9909 (0.0009)
EW3D	150	0.0301 (0.0003)	0.9949 (0.0008)
EW3D	200	0.0214 (0.0002)	0.9945 (0.0005)
EW3D	300	0.0135 (0.0002)	0.9967 (0.0009)
EW3DC	100	0.0000 (0.0003)	0.9972 (0.0005)

[a]EW3D and EW3DC refer to Ewald summation methods without and with the correction term for the planar vacuum boundary condition, respectively. Errors in parentheses were based on the 95% confidence interval estimated as 1.96 times the standard error. Standard errors were estimated from an analysis of five equal time blocks from the trajectory of each production run. $\langle\cos\theta_{dipole,z}\rangle$ values are the average values of cosine of the angle between the water dipole and the z-axis.

2. Electrostatic properties

To investigate the unusual orientational ordering of water molecules in simulations with the EW3D method, we calculated electrostatic properties across the quartz/water interface. Figures 4(a) and 4(b), show profiles of the electrostatic potential and electric field calculated by applying Eqs. (13) and (14), compatible with the planar vacuum boundary con-

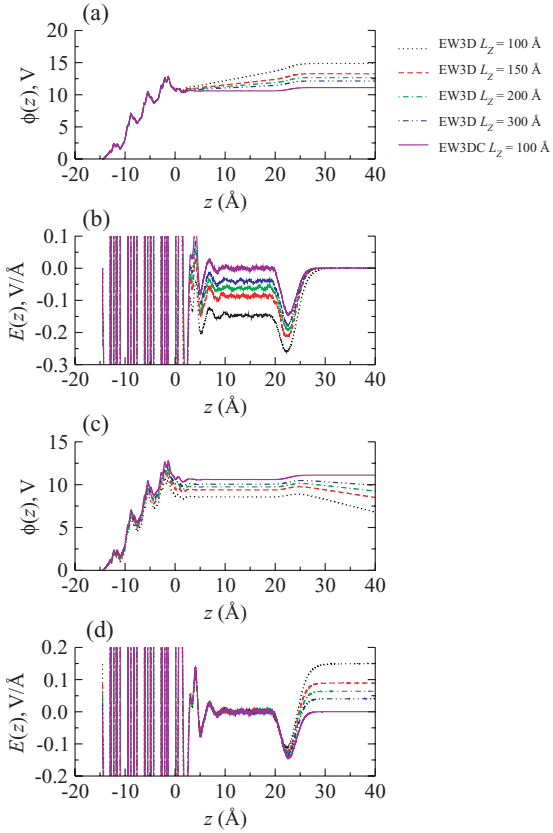

FIG. 4. Electrostatic properties of the quartz/water interface. (a) and (b) Profiles of electrostatic potential [$\phi(z)$] and electric field [$E(z)$], respectively, calculated by applying Eqs. (13) and (14) suitable for the planar vacuum boundary condition to simulation data generated under the conducting periodic boundary condition (EW3D). (c) and (d) The same profiles are calculated by applying Eqs. (11) and (12), i.e., applying the consistent conducting periodic boundary condition to both the simulation (EW3D) and the calculation of electrostatic properties. All results from simulations performed and analyzed using the planar vacuum boundary condition with the periodic boundary condition correction (EW3DC) are shown as solid lines and were obtained by using Eqs. (13) and (14).

dition. In this case, the electrostatic potential increased with increasing z in the bulklike water region, resulting in negative electric field values, which were not consistent with the positive $\langle \cos \theta_{\text{dipole},z} \rangle$ values shown in Fig. 3(b). Figures 4(c) and 4(d), show the results obtained by applying formulas appropriate to the electrostatic boundary conditions used in the simulations, namely, Eqs. (11) and (12) for simulations using the conducting boundary condition (EW3D) and Eqs. (13) and (14) for the simulation using the planar vacuum boundary condition (EW3DC). The electrostatic potential profile obtained with the EW3D method was nearly flat in the region occupied by the bulklike water, resulting in near zero but slightly positive electric field values, consistent with the positive $\langle \cos \theta_{\text{dipole},z} \rangle$ values shown in Fig. 3(b). However, these relatively weak electrostatic fields were not strong enough to alter the density distributions of water molecules embedded on the hydrogen-bonded network of the liquid water phase. In contrast, the average electric field in the region with the bulklike water density with the EW3DC method was close to zero, also consistent with the $\langle \cos \theta_{\text{dipole},z} \rangle$ values shown in Fig. 3(b) and Table I. This also demonstrates that the smallest box size of 100 Å was large enough to obtain correct electrostatic properties when we use the proper correction term for the planar vacuum boundary condition, as implemented in the EW3DC method.

Gurtovenko and Vattulainen[32] claimed that using Eq. (12), derived for conducting boundary conditions, for simulation systems with nonzero net dipole moments is not appropriate even if the simulations are performed with the conducting boundary condition. Instead, they suggested using Eq. (14), which was derived for the planar vacuum boundary condition. However, our results in Figs. 3 and 4 clearly show that self-consistent electrostatic properties can be obtained only if we use the formula corresponding to the electrostatic boundary condition used in the simulation.

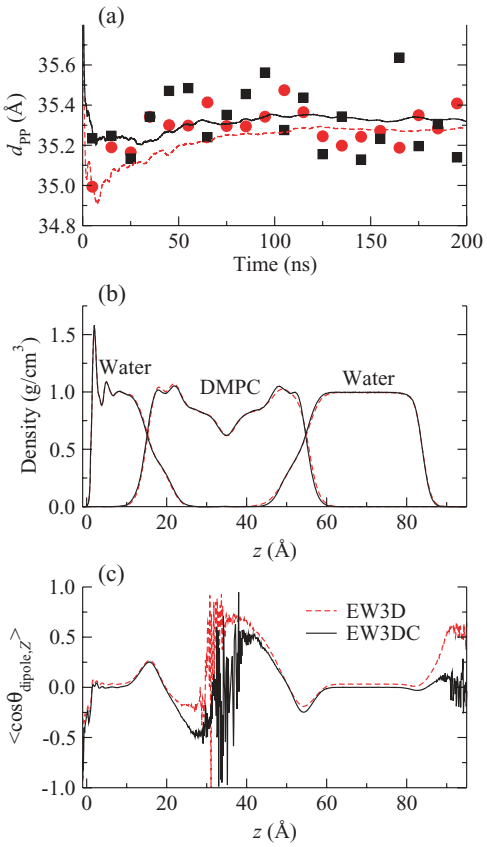

FIG. 5. Structural properties of the quartz-supported DMPC lipid bilayer. (a) d_{PP}, the average distance between phosphate atoms in upper and lower leaflets, as a function of time. Circles and squares represent 10-ns block averages for simulations with the EW3D and EW3DC methods, respectively. Dashed and solid lines represent cumulative averages for the EW3D and EW3DC methods, respectively. (b) Distributions of mass density contributed by the DMPC lipid bilayer and water molecules calculated from simulations with the EW3D (dashed lines) and EW3DC (solid lines) methods. (c) Comparison of $\langle \cos \theta_{\text{dipole},z} \rangle$ values obtained from simulations with the EW3D (dashed lines) and EW3DC (solid lines) methods.

B. Hydrated DMPC bilayer on the quartz crystal

1. Structural properties

Figure 5(a) shows the thickness of the DMPC bilayer represented by d_{PP}, the average distance between phosphate atoms in upper and lower leaflets, as a function of time. Both 10-ns block and cumulative averages of d_{PP} show that the simulated systems relaxed within 70 ns, our choice of the equilibration time. Figure 5(b) shows the contributions to the mass density distributions by DMPC and water across the hydrated DMPC bilayer deposited on the quartz crystal. Density distributions calculated from simulations using either the EW3D or EW3DC methods were quite similar. Density distributions of water between the quartz surface and the DMPC bilayer at 0 Å $< z <$25 Å were influenced by interactions with both the quartz and the DMPC bilayer. On the other hand, the thicker water layer between the DMPC bilayer and vacuum phase contained a significant bulklike region between $z = 65$ and 75 Å.

Figure 5(c) shows the values of $\langle \cos \theta_{\text{dipole},z} \rangle$ as a function of the distance from the quartz surface and demonstrates that when water molecules approach the lipid bilayer from the bulk phase, the water dipole initially points toward the membrane at the interfaces (8.4 Å $< z <$ 19.3 Å or 50.2 Å $< z <$ 61.9 Å). For water molecules penetrating further into the membrane (19.3 Å $< z <$ 50.2 Å), their dipole points away from the membrane center. As observed for waters in the pure quartz/water system, water molecules in the simulations with the EW3D method were more polarized compared with those with the EW3DC method even in the bulklike region.

2. Electrostatic properties

Figure 6 shows electrostatic properties calculated for the hydrated DMPC bilayer supported on the quartz crystal. As shown in Fig. 6(a), the electrostatic potential dropped noticeably across the membrane region and the vacuum phase with the EW3D method, resulting in a larger electric field [as shown in Fig. 6(b)] compared with those obtained with the EW3DC method. At a first glance, these potential drops across the membrane region and vacuum region may seem physically unreasonable. However, this is a real consequence of having PBCs under the conducting boundary condition. An increased potential in one part of the system (a polarized crys-

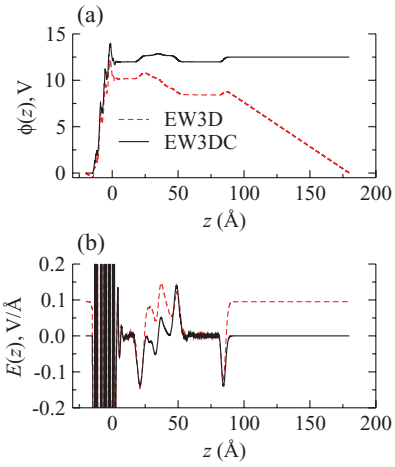

FIG. 6. Electrostatic properties of the quartz-supported DMPC lipid bilayer. (a) and (b) Profiles of $\phi(z)$ and $E(z)$ with the EW3D (dashed lines) and EW3DC (solid lines) methods.

tal in this case) has to be compensated for elsewhere to satisfy the imposed PBCs.

The average electric field near the region occupied by the bulklike water between DMPC bilayer and the water/vacuum interface between $z = 65$ and 75 Å in simulations with the EW3D method had a slight positive value of 0.95 ($\pm$0.15) mV/Å. With the polarization P_z in the z-direction estimated from the $\langle \cos \theta_{\text{dipole},z} \rangle$ value in the bulklike region of water in Fig. 5(b), we can estimate the dielectric constant ε of water by the following relation:

$$\varepsilon = 1 + \frac{P_z}{\varepsilon_0 E}. \tag{15}$$

The estimated value of ε was 103 ($\pm$17), in close agreement with the value of 94 obtained from a series of simulations of TIP3P bulk water with different electric fields.[36] This confirms that Eq. (11) produces an electric field consistent with the observed orientational polarization of water in simulations performed with the EW3D method.

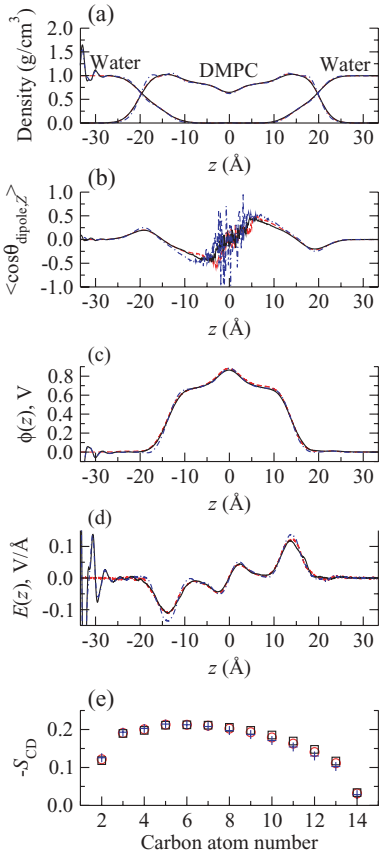

FIG. 7. Comparison of DMPC lipid bilayers in solution (dashed lines) and with the quartz/water interface (solid lines) with a larger system size having 176 lipids. Dotted-dashed lines represent the results with the original system size having 44 lipids. Distributions with the quartz/water interface were shifted with respect to the membrane center to coincide with the free solvated bilayer. (a) Distributions of mass density contributed by DMPC lipids and water molecules. (b) $\langle \cos \theta_{\text{dipole},z} \rangle$ values across the interface. (c) $\phi(z)$ values. (d) $E(z)$ values. (e) Order parameter of acyl chain *sn*-1 calculated by $S_{\text{CD}} = \left\langle \frac{3\cos^2\theta - 1}{2} \right\rangle$, where θ is the angle between the C–H vector and the z-axis. Circles and squares represent results with a larger system size for DMPC bilayers in solution and with the quartz/water interface, respectively. Pluses represent the results with the original system size.

C. Comparison of bilayers in solution and at the quartz/water interface

We compared structural and electrostatic properties of the DMPC bilayer solvated in bulk water and near the quartz/water interface. Simulations with a larger system size having 176 lipids were used for a more realistic comparison. The results from the EW3DC simulation with the original system size shown in Figs. 5 and 6 were also compared. Figure 7 shows the results of this comparison. Distributions for the solid-supported bilayer were shifted with respect to the average membrane center to facilitate comparisons with the bulk simulation. Figure 7(a) shows that the contributions to the mass density distribution from DMPC were similar in bulk water and near the quartz/water interface. Mass density distributions of water were also similar even though they fluctuated around the bulk density near the quartz surface. Figures 7(b)–7(e) show the comparisons of the profiles of polarization of water, electrostatic potential, electric field, and lipid acyl chain order parameter,[37] respectively, in bulk solution, in the presence of the quartz/water interface, and with a smaller system size. Even though small differences existed, the properties across the bilayers were, overall, very similar. These results demonstrated that a quartz-supported lipid bilayer deposited on top of a thin water film does not introduce any gross differences to a completely solvated bilayer. Thus, the simulations indicate that the deposited bilayer could be an equivalent model to study the properties of a lipid bilayer in solution. However, the properties of lipid bilayers could be affected if a thinner water layer between the solid support and the lipid bilayer is modeled as suggested by experiments[9] and simulations.[11] Most importantly, with the rigorous treatment of electrostatic boundary conditions developed in this study for the quartz-supported lipid bilayer, a variety of lipid/cholesterol/peptide/protein interactions with membranes can now be accurately simulated while preserving the inherent anisotropy of the system.

D. Quartz/water interface in bulk solution

The planar vacuum boundary condition or the EW3DC method is commonly applied to simulations of interfacial systems embedded in vacuum such as the quartz/water interface or the solid-supported lipid bilayer described above. However, the P_z/ε_0 term in Eq. (11) is applicable to any simulations performed under conducting boundary conditions, regardless whether the simulated system is in bulk solution or embedded in vacuum. Therefore, we investigated whether artificial PBC-induced orientational ordering was present for a fully solvated quartz interface using conducting boundary conditions and how it can be removed by implementing the EW3DC planar vacuum boundary condition. Figures 8(a) and 8(b), show a comparison of distributions of mass density and orientational polarization of water, respectively, across the quartz/water interface in bulk solution obtained from simulations with the EW3D and EW3DC methods. Density distributions of water near the hydrophilic side ($z > 7$ Å) of the quartz crystal for both methods were similar to those shown in Fig. 3(a) for the quartz/water interface embedded in vacuum. However, the unusual ordering of water with the EW3D method using the conducting boundary condition in Fig. 8(b) was more pronounced compared with when embedded in vacuum. In addition, the water density distribution near the hydrophobic side ($z < -7$ Å) in Fig. 8(a) was also affected by the choice of the electrostatic boundary condition due to the high degree of ordering of water with the EW3D method. The distribution of water density near the hydrophobic side was also slightly different compared with that obtained from a previous simulation[26] where electrostatic interactions were truncated. As expected, the unusual ordering of water was completely removed when we used the planar vacuum boundary condition with the EW3DC method. Distributions of the electrostatic potential and electric field shown in Figs. 8(c) and 8(d), calculated with formulas corresponding to the employed boundary condition, were consistent with the $\langle \cos \theta_{\mathrm{dipole},z} \rangle$ values shown in Fig. 8(b). A similar relationship between $\langle \cos \theta_{\mathrm{dipole},z} \rangle$ and the electric field was observed in the previous simulation of TIP3P bulk water.[36] Our results demonstrate that the planar vacuum boundary condition can be applied to more general interfacial systems in bulk solution to remove the nonphysical ordering observed under the conducting boundary condition.

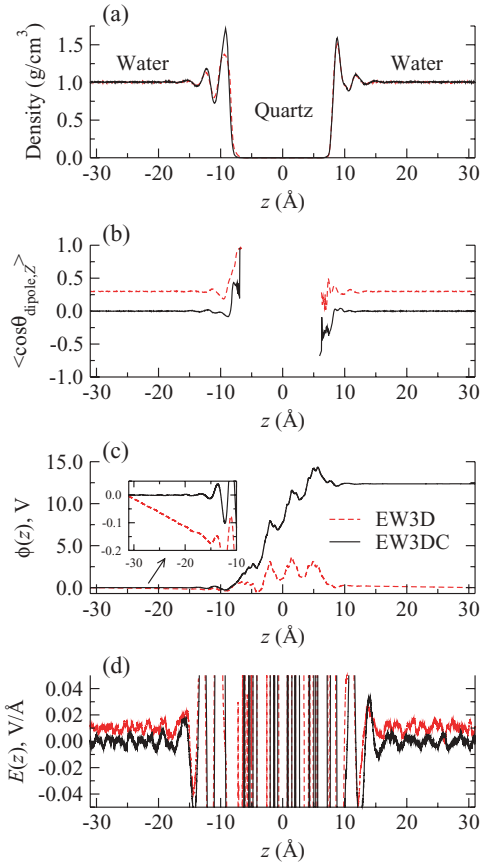

FIG. 8. Structural and electrostatic properties of the quartz/water interface in bulk solution without vacuum interfaces. Results with the EW3D and EW3DC methods are shown by the dashed and solid lines, respectively. Distributions were calculated with respect to the center of the quartz crystal. (a) Distributions of mass density contributed by water molecules. (b) $\langle \cos \theta_{\mathrm{dipole},z} \rangle$ values across the interface. (c) $\phi(z)$ values. (d) $E(z)$ values. The *inset* in *C* shows a magnified view of $\phi(z)$ profiles in the bulklike region of the water phase.

IV. SUMMARY AND CONCLUSIONS

The general system consisting of a solvated bilayer adsorbed on a solid surface and exposed to an air/vacuum interface occurs in many experimental settings and presents some unique computational challenges. In this study, we examined how the structural and electrostatic properties of polarized interfacial systems are affected by the choice of the electrostatic boundary condition and the importance of analyzing electrostatic properties with the correct formulas corresponding to the deployed boundary conditions. We showed that implementing the standard Ewald summation with the conducting boundary condition for interfacial systems with a net polarization introduced an abnormal orientational polarization of water. Our analyses suggest that the polarized component in the simulated system (e.g., a polarized quartz crystal or an asymmetric bilayer) affects the properties of other parts of the system by a compensation mechanism when we apply the conducting boundary condition. Implementing the Ewald summation technique with the planar vacuum boundary condition and evaluating electrostatic properties with formulas corresponding to the electrostatic boundary condition does not introduce any such compensatory effect, and the influence of the polarized component is more realistically accounted for. We also confirmed that the modeled quartz-supported hydrated lipid bilayer reproduced the essential features of the lipid bilayer in bulk water.

ACKNOWLEDGMENTS

We thank Dr. Ramanathan Nagarajan and Dr. Hyung-June Woo for their helpful suggestions and discussions. This project was funded in part by a competitive In-house Laboratory Independent Research (ILIR) grant by the U.S. Army Assistant Secretary of the Army for Acquisition, Logistics, and Technology (ASAALT). Funding support for this work also came from the Department of Defense (DoD) High

Performance Computing (HPC) Modernization Program Office, under the HPC Software Applications Institute initiative, the U.S. Army Medical Research and Materiel Command. Computational time was provided by the U.S. Army Research Laboratory and Navy DoD Supercomputing Resource Centers. The opinions or assertions contained herein are the private views of the authors and are not to be construed as official or as reflecting the views of the U.S. Army or of the U.S. Department of Defense. This paper has been approved for public release.

[1]B. Honig and A. Nicholls, Science **268**(5214), 1144 (1995); N. Sinha and S. J. Smith-Gill, Curr. Protein Pept. Sci. **3**(6), 601 (2002); P. Koehl, Curr. Opin. Struct. Biol. **16**(2), 142 (2006); K. D. Collins, G. W. Neilson, and J. E. Enderby, Biophys. Chem. **128** (2–3), 95 (2007).
[2]M. P. Allen and D. J. Tildesley, *Computer Simulation of Liquids* (Oxford University Press, New York, 1987).
[3]P. Ewald, Ann. Phys. **64**, 253 (1921).
[4]L. Greengard and V. Rokhlin, J. Comput. Phys. **73**(2), 325 (1987); J. Lekner, Physica A **176**, 485 (1991); X. Wu and B. R. Brooks, J. Chem. Phys. **122**(4), 044107 (2005).
[5]S. W. de Leeuw, J. W. Perram, and E. R. Smith, Proc. R. Soc. London, Ser. A **373**, 27 (1980).
[6]S. W. de Leeuw, J. W. Perram, and E. R. Smith, Proc. R. Soc. London, Ser. A **388**, 177 (1983).
[7]T. A. Darden, D. M. York, and L. G. Pedersen, J. Chem. Phys. **98**, 10089 (1993); U. Essmann, L. Perera, M. L. Berkowitz, T. Darden, H. Lee, and L. G. Pedersen, J. Chem. Phys. **103**, 8577 (1995).
[8]M. Karttunen, J. Rottler, I. Vattulainen, C. Sagui, and E. F. Scott, *Current Topics in Membranes* (Academic, New York, 2008), Vol. 60, p. 49.
[9]C. E. Miller, J. Majewski, T. Gog, and T. L. Kuhl, Phys. Rev. Lett. **94**(23), 238104 (2005); E. B. Watkins, C. E. Miller, D. J. Mulder, T. L. Kuhl, and J. Majewski, Phys. Rev. Lett. **102**(23), 238101 (2009); T. H. Anderson, Y. J. Min, K. L. Weirich, H. B. Zeng, D. Fygenson, and J. N. Israelachvili, Langmuir **25**(12), 6997 (2009).
[10]D. R. Heine, A. R. Rammohan, and J. Balakrishnan, Mol. Simul. **33**(4–5), 391 (2007); S. V. Bennun, A. N. Dickey, C. Y. Xing, and R. Faller, Fluid Phase Equilib. **261**(1–2), 18 (2007); C. Y. Xing and R. Faller, J. Phys. Chem. B **112**(23), 7086 (2008); C. Y. Xing, O. H. S. Ollila, I. Vattulainen, and R. Faller, Soft Matter **5**(17), 3258 (2009); C. Y. Xing and R. Faller, *ibid*. **5**(22), 4526 (2009); C. Y. Xing and R. Faller, J. Chem. Phys. **131**(17), 175104 (2009); M. I. Hoopes, M. Deserno, M. L. Longo, and R. Faller, J. Chem. Phys. **129**(17), 175102 (2008).
[11]M. Roark and S. E. Feller, Langmuir **24**(21), 12469 (2008); S. V. Bennun, M. I. Hoopes, C. Y. Xing, and R. Faller, Chem. Phys. Lipids **159**(2), 59 (2009); M. I. Hoopes, C. Xing, and R. Faller, *Biomembrane Frontiers*, edited by R. Faller, M. L. Longo, S. H. Risbud, and T. Jue (Humana, New York, 2009), p. 101.
[12]S. E. Feller, R. W. Pastor, A. Rojnuckarin, S. Bogusz, and B. R. Brooks, J. Phys. Chem. **100**, 17011 (1996); I.-C. Yeh and M. L. Berkowitz, J. Chem. Phys. **110**(16), 7935 (1999).
[13]J. C. Shelley and G. N. Patey, Mol. Phys. **88**, 385 (1996).
[14]E. R. Smith, Proc. R. Soc. London, Ser. A **375**, 475 (1981).
[15]H. D. Herce, A. E. Garcia, and T. Darden, J. Chem. Phys. **126**(12), 124106 (2007); B. P. van Eijck and J. Kroon, J. Phys. Chem. B **101**(6), 1096 (1997).
[16]I.-C. Yeh and M. L. Berkowitz, J. Chem. Phys. **111**(7), 3155 (1999).
[17]D. E. Parry, Surf. Sci. **54**, 195 (1976); D. M. Heyes, M. Barber, and J. H. R. Clarke, J. Chem. Soc., Faraday Trans. 2 **73**, 1485 (1977); E. Spohr, J. Chem. Phys. **107**, 6342 (1997).
[18]J. Janeček and R. R. Netz, Langmuir **23**(16), 8417 (2007).
[19]V. Buch, A. Milet, R. Vacha, P. Jungwirth, and J. P. Devlin, Proc. Natl. Acad. Sci. U.S.A. **104**(18), 7342 (2007); D. Bostick and M. L. Berkowitz, Biophys. J. **85**(1), 97 (2003).
[20]J. N. Sachs, P. S. Crozier, and T. B. Woolf, J. Chem. Phys. **121**(22), 10847 (2004).
[21]I.-C. Yeh and G. Hummer, Proc. Natl. Acad. Sci. U.S.A. **101**(33), 12177 (2004).
[22]K. A. Marx, Biomacromolecules **4**(5), 1099 (2003).
[23]L. Kale, R. Skeel, M. Bhandarkar, R. Brunner, A. Gursoy, N. Krawetz, J. Phillips, A. Shinozaki, K. Varadarajan, and K. Schulten, J. Comput. Phys. **151**(1), 283 (1999).
[24]A. D. MacKerell, D. Bashford, M. Bellott, R. L. Dunbrack, J. D. Evanseck, M. J. Field, S. Fischer, J. Gao, H. Guo, S. Ha, D. Joseph-McCarthy, L. Kuchnir, K. Kuczera, F. T. K. Lau, C. Mattos, S. Michnick, T. Ngo, D. T. Nguyen, B. Prodhom, W. E. Reiher, B. Roux, M. Schlenkrich, J. C. Smith, R. Stote, J. Straub, M. Watanabe, J. Wiorkiewicz-Kuczera, D. Yin, and M. Karplus, J. Phys. Chem. B **102**(18), 3586 (1998).
[25]W. L. Jorgensen, J. Chandrasekhar, J. D. Madura, R. W. Impey, and M. L. Klein, J. Chem. Phys. **79**, 926 (1983).
[26]P. E. M. Lopes, V. Murashov, M. Tazi, E. Demchuk, and A. D. MacKerell, J. Phys. Chem. B **110**(6), 2782 (2006).
[27]J. P. Ryckaert, G. Ciccotti, and H. J. C. Berendsen, J. Comput. Phys. **23**, 327 (1977).
[28]I. C. Yeh and A. Wallqvist, J. Phys. Chem. B **113**(36), 12382 (2009).
[29]S. Jo, T. Kim, V. G. Iyer, and W. Im, J. Comput. Chem. **29**(11), 1859 (2008).
[30]H. I. Petrache, S. W. Dodd, and M. F. Brown, Biophys. J. **79**(6), 3172 (2000).
[31]B. R. Brooks, R. E. Bruccoleri, B. D. Olafson, D. J. States, S. Swaminathan, and M. Karplus, J. Comput. Chem. **4**, 187 (1983); B. R. Brooks, C. L. Brooks, A. D. Mackerell, L. Nilsson, R. J. Petrella, B. Roux, Y. Won, G. Archontis, C. Bartels, S. Boresch, A. Caflisch, L. Caves, Q. Cui, A. R. Dinner, M. Feig, S. Fischer, J. Gao, M. Hodoscek, W. Im, K. Kuczera, T. Lazaridis, J. Ma, V. Ovchinnikov, E. Paci, R. W. Pastor, C. B. Post, J. Z. Pu, M. Schaefer, B. Tidor, R. M. Venable, H. L. Woodcock, X. Wu, W. Yang, D. M. York, and M. Karplus, *ibid*. **30**(10), 1545 (2009).
[32]A. A. Gurtovenko and I. Vattulainen, J. Chem. Phys. **130**(21), 215107 (2009).
[33]M. C. F. Wander and A. E. Clark, J. Phys. Chem. C **112**(50), 19986 (2008).
[34]S. H. Lee and P. J. Rossky, J. Chem. Phys. **100**(4), 3334 (1994).
[35]R. S. Neves, A. J. Motheo, R. P. S. Fartaria, and F. Fernandes, J. Electroanal. Chem. **612**(2), 179 (2008); F. Goujon, C. Bonal, B. Limoges, and P. Malfreyt, Langmuir **25**(16), 9164 (2009).
[36]I.-C. Yeh and G. Hummer, Biophys. J. **86**(2), 681 (2004).
[37]L. S. Vermeer, B. L. de Groot, V. Reat, A. Milon, and J. Czaplicki, Eur. Biophys. J. **36**(8), 919 (2007).